

Verification of satellite and model products against a dense rain gauge network for a severe flooding event in Kumasi, Ghana

Article

Published Version

Creative Commons: Attribution 4.0 (CC-BY)

Open Access

Agyekum, J. ORCID: <https://orcid.org/0000-0001-7484-5338>, Amekudzi, L. K., Stein, T. ORCID: <https://orcid.org/0000-0002-9215-5397>, Aryee, J. N. A., Atiah, W. A., Adefisan, E. A. ORCID: <https://orcid.org/0000-0003-3339-5195> and Danuor, S. K. (2023) Verification of satellite and model products against a dense rain gauge network for a severe flooding event in Kumasi, Ghana. *Meteorological Applications*, 30 (5). e2150. ISSN 1469-8080 doi: 10.1002/met.2150 Available at <https://centaur.reading.ac.uk/113555/>

It is advisable to refer to the publisher's version if you intend to cite from the work. See [Guidance on citing](#).

To link to this article DOI: <http://dx.doi.org/10.1002/met.2150>

Publisher: Wiley

All outputs in CentAUR are protected by Intellectual Property Rights law, including copyright law. Copyright and IPR is retained by the creators or other copyright holders. Terms and conditions for use of this material are defined in the [End User Agreement](#).

www.reading.ac.uk/centaur




CentAUR

Central Archive at the University of Reading

Reading's research outputs online

RESEARCH ARTICLE

Verification of satellite and model products against a dense rain gauge network for a severe flooding event in Kumasi, Ghana

Jacob Agyekum^{1,2}  | Leonard K. Amekudzi¹ | Thorwald Stein³  |
 Jeffrey N. A. Aryee¹ | Winifred Ayinpogbilla Atiah¹ |
 Elijah Adesanya Adefisan⁴  | Sylvester K. Danuor⁵

¹Department of Meteorology and Climate Science, Kwame Nkrumah University of Science and Technology, Kumasi, Ghana

²Water Research Institute, Council for Scientific and Industrial Research, Accra, Ghana

³Department of Meteorology, University of Reading, Reading, UK

⁴African Centre of Meteorological Applications for Development (ACMAD), Niamey, Niger

⁵Department of Physics, Kwame Nkrumah University of Science and Technology, Kumasi, Ghana

Correspondence

Jacob Agyekum, Department of Meteorology and Climate Science, Kwame Nkrumah University of Science and Technology, Kumasi, Ghana.

Email: jacobyff@gmail.com

Funding information

UK Research and Innovation as part of the Global Challenges Research Fund, Grant/Award Number: NE/P021077/1

Abstract

Floods as a result of severe storms cause significant impacts on lives and properties. Therefore, timely and accurate forecasts of the storms will reduce the associated risks. In this study, we look at the characteristics of a storm on 28 June, 2018 in Kumasi from a rain gauge network and satellite data, and reanalysis data. The storm claimed at least 8 lives and displaced 293 people in Kumasi, Ghana. The ability of satellite and reanalysis data to capture the temporal variations of the storm was assessed using a high temporal resolution (accumulation per minute) rain gauge data. We employed the observation data from the Dynamics–Aerosol–Chemistry–Cloud Interactions in West Africa (DACCIWA) rain gauges to assess the storm's onset, duration, and cessation. Subsequently, the performance of the ERA5 reanalysis and Global Precipitation Measurement (GPM) satellite precipitation estimates in capturing the rainfall is assessed. Both GPM and the ERA5 had difficulty reproducing the hourly pattern of the rain. However, the GPM produced variability that is similar to the observed. Generally, the region of maximum rainfall was located in the southern parts of the study domain in ERA5, while GPM placed it in the northern parts. The study contributes a verification measure to improve weather forecasting in Ghana as part of the objectives of the GCRF African Science for Weather Information and Forecasting Techniques (SWIFT) project.

KEYWORDS

Ghana, rain gauge, satellite, verification, weather extremes

1 | INTRODUCTION

Weather forecasting is an essential service that informs the planning of socioeconomic activities (Inness &

Dorling, 2012). Accuracy in weather prediction has helped prevent the loss of lives and properties (Murray, 2018). For instance, the Ghana Meteorological Agency (GMet) has issued forecasts that saved farmers from huge losses over

This is an open access article under the terms of the [Creative Commons Attribution](https://creativecommons.org/licenses/by/4.0/) License, which permits use, distribution and reproduction in any medium, provided the original work is properly cited.

© 2023 The Authors. *Meteorological Applications* published by John Wiley & Sons Ltd on behalf of Royal Meteorological Society.

the years. These include daily and seasonal forecasts given by GMet to the general public and farmers regarding the onset, duration, and cessation of the country's rainfall season (Ansah et al., 2020). The seasonal forecast has improved farming in Ghana by enabling farmers to know the exact periods for land preparation and crop planting. Crop losses resulting from inadequate rainfall have reduced drastically (Antwi-Agyei et al., 2012; Owusu & Waylen, 2013). Meteorological observations are critical for producing accurate weather forecasts, establishing efficient early warning systems, and monitoring climate change (Karley, 2009; Mudombi & Nhamo, 2014). However, these observations are sparse in Africa, particularly lack of dense rain gauge networks needed for calibration and validation of satellite products (Dinku et al., 2011; Thorne et al., 2001; Wood et al., 2000).

Globally and regionally, storms, such as hurricanes, severe thunderstorms, and extreme heat events cause significant damage to buildings, roads, and farms. These damages subsequently have impacts on the socioeconomic activities of most countries. In Ghana, Accra and Kumasi, over the years, have frequently been devastated by floods (Karley, 2009). Prominent among these is 3 June, 2015, when heavy and continuous rainfall caused flooding in Accra and neighboring towns (Asumadu-Sarkodie et al., 2015; Tengan & Aigbavboa, 2016). The floods coupled with a fueling station explosion claimed over 150 lives and destroyed properties valued at over \$428,000 (Asumadu-Sarkodie et al., 2015). The rains started late afternoon and lasted for over 6 h (Asumadu-Sarkodie et al., 2015). Although GMet issued a weather warning for this event, they did not accurately forecast the storm's duration and intensity.

Weather forecasters often rely on data from current observations and numerical weather prediction (NWP) models to help assess prevailing atmospheric conditions, such as those that may lead to thunderstorms. Convection-permitting NWP models significantly improve the representation of thunderstorms over the tropics (Finney et al., 2019; Stratton et al., 2018). However, these models require high computational resources, primarily unavailable in most African meteorological centers. Additionally, models need observation data to provide quality weather forecasts. Over the years, studies have supported storm identification over West Africa. Some have used NWPs (Done et al., 2004; Sieglaff et al., 2011; Sun et al., 2014), satellite (Banta & Barker Schaaf, 1987; Browning et al., 2007; Sieglaff et al., 2011), and radar (Dixon & Wiener, 1993; Goudenhoofd & Delobbe, 2013; Wilson & Schreiber, 1986) to identify storms' characteristics. Geostationary satellite images have beneficial uses for tracking storm initiations (Sieglaff et al., 2011), needed for creating convective initiation nowcasts based on a combination of cloud-top cooling rates and satellite-derived cloud-top type-phase trends. Other studies have employed a combination of

satellite and rain gauge data for storm tracking and nowcasting (Maranan et al., 2020; Nesbitt et al., 2004). The fidelity of satellites as well as other rainfall estimates in capturing observed rainfall will improve storm tracking for early warning systems. Evaluating satellite rainfall estimates (SREs) from daily to annual scale, Ageet et al. (2022) showed the robustness of SREs in reproducing the seasonal and annual patterns of rainfall over equatorial East Africa. They specifically indicated the skill of Integrated Multi-satellite Retrievals for GPM (IMERG) in reproducing the daily rainfall estimates. A similar evaluation study over Ghana by Atiah, Amekudzi, et al. (2020) assessed the ability of satellite and satellite merged with gauge data to ascertain their skill in reproducing rainfall climatologies. Amekudzi et al. (2016) evaluated Tropical Rainfall Measuring Mission (TRMM) and Famine Early Warning System (FEWS) satellite estimates over the Ashanti Region of Ghana employing various statistical methods. They indicated the robustness of both datasets in reproducing the onset, peak, and cessation of the rainy season.

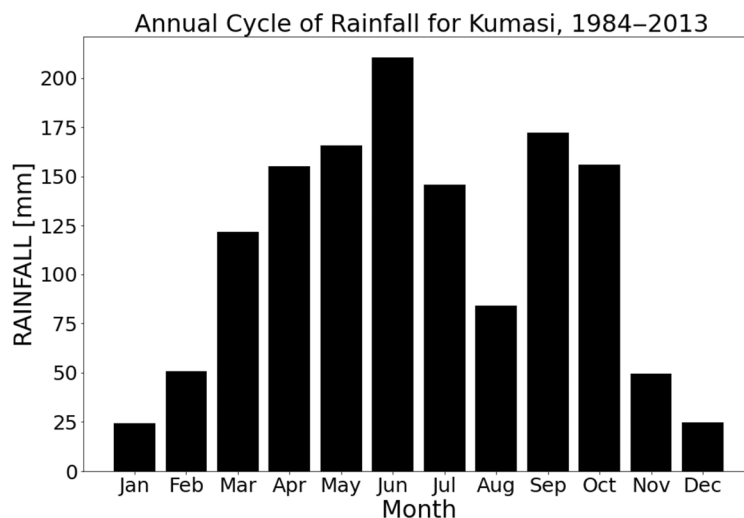
Existing studies have focused mainly on validating the skill of rainfall estimates on daily to annual scales over Ghana and West Africa at large. Partly due to the unavailability of long-term sub-daily rain gauge data in the region. Using high temporal resolution data (sub-daily) is crucial for meteorological applications by providing the opportunity to track and analyze the initiation, duration, and intensities of storms and data for model evaluation. A recent study by Maranan et al. (2020) assessed the performance of Integrated Multi-satellite Retrievals for Global Precipitation Measurement (GPM), version 6b (IMERG), using the DACCWA rain gauge network over the Ashanti Region of Ghana. The work showed the skill of IMERG in reproducing 2-year (2016–2017) precipitation. The DACCWA rain gauge network over the Ashanti Region of Ghana recording rainfall accumulation every minute provides data for ascertaining storm characteristics and evaluating rainfall products at the sub-daily timescale. Consequently, this study is built on previous evaluation studies and offers a first-hand look at the use of highly resolved (rainfall accumulation per minute) observation data to assess the characteristics of an extreme rainfall event in Kumasi, a town in Ghana. This study aims to describe the synoptic conditions leading up to the heavy rainfall event (on 28 June, 2018) and to verify the capability of GPM and ERA5 reanalysis to capture the duration and intensity of the event.

2 | DATA AND METHODS

2.1 | Study area

Kumasi is the capital of the Ashanti Region located in south-central Ghana (6°36' N–6°41' N, 1°42' W–1°30' W).

FIGURE 1 Climatological mean of annual cycle of rainfall over Kumasi for the 1984–2013 period based on daily rain gauge data (Data from Ghana Meteorological Agency).



W). The climate is tropical, characterized by a bimodal annual rainfall cycle, with the major rainy season spanning from April to June and the minor season spanning from September and October (Figure 1) (Amekudzi et al., 2016; Atiah, Tsidu, et al., 2020). Mean annual rainfall and temperature are respectively, 1300 mm (Aryee et al., 2018; Nero et al., 2017) and 26.4°C (Quansah et al., 2014). The dry and wet seasons are regulated by the meridional movement of the inter-tropical discontinuity (ITD) and the St. Helena and Azores high-pressure systems (Ansah et al., 2020; Manzananas et al., 2014). The intensification of the St. Helena High during the wet season (April, May, June, and July) enhances the influx of moisture in the country through the southwesterly wind. In the dry season, the Azores High intensifies and enhances the inflow of dust from the Sahara through the northeasterly winds.

2.2 | Rain gauge data

The DACCWA was a European Union seventh framework funded project with a prime mandate of investigating the influence of anthropogenic and natural emissions on the atmospheric composition over South West Africa and assessing their impact on human and ecosystem health and agricultural productivity (Knippertz et al., 2015). As part of this project, 17 optical rain gauges with 1-min temporal resolutions were deployed over the Ashanti Region of Ghana. Some of the rain gauges are still operational to date. The measuring technique of the DACCWA optical gauges is such that rainfall collected into the optical gauge's collector is detected and counted by a sensor in the optical gauge's logger. The optical gauge works with the principle that any raindrop through its collector assumes the size of its orifice. The rainfall event can therefore be inferred in Equation (1).

$$R = r * Nd, \quad (1)$$

where R is the rainfall amount, r is the constant radius of the orifice (0.01 mm), and Nd represents the number of raindrops. For this study, 14 gauges were available, providing dense coverage in the center of Ashanti (see Figure 2). DACCWA gauge data will be referred to as the gauge observation or gauges hereafter.

2.3 | Integrated Multi-satellite Retrievals for GPMs

IMERG is a joint mission between the Japan Aerospace Exploration Agency (JAXA) and the National Aeronautics and Space Administration (NASA). The IMERG, which has been operational since 2014, provides global observations of rainfall and snow at temporal resolutions of 30 min, 3 hourly, and daily and spatial resolution of $0.1^\circ \times 0.1^\circ$ (Huffman, Bolvin, Braithwaite, et al., 2015; Huffman, Bolvin, Nelkin, et al., 2015). The IMERG can be used as a reference for areas where rain gauges are sparse or not available (Gilewski & Nawalany, 2018; Ramsauer et al., 2018). The final version of hourly accumulations for 28 June, 2018 was used for this study.

2.4 | European Centre for Medium-Range Weather Forecast (ECMWF) reanalysis; ERA-INTERIM and ERA5

The ERA5 and ERA-INTERIM atmospheric profile data were used to assess the atmospheric stability. First, the ability of ERA5 and ERA-INTERIM to reproduce in situ atmospheric profile measurements on the 17 June, 2016

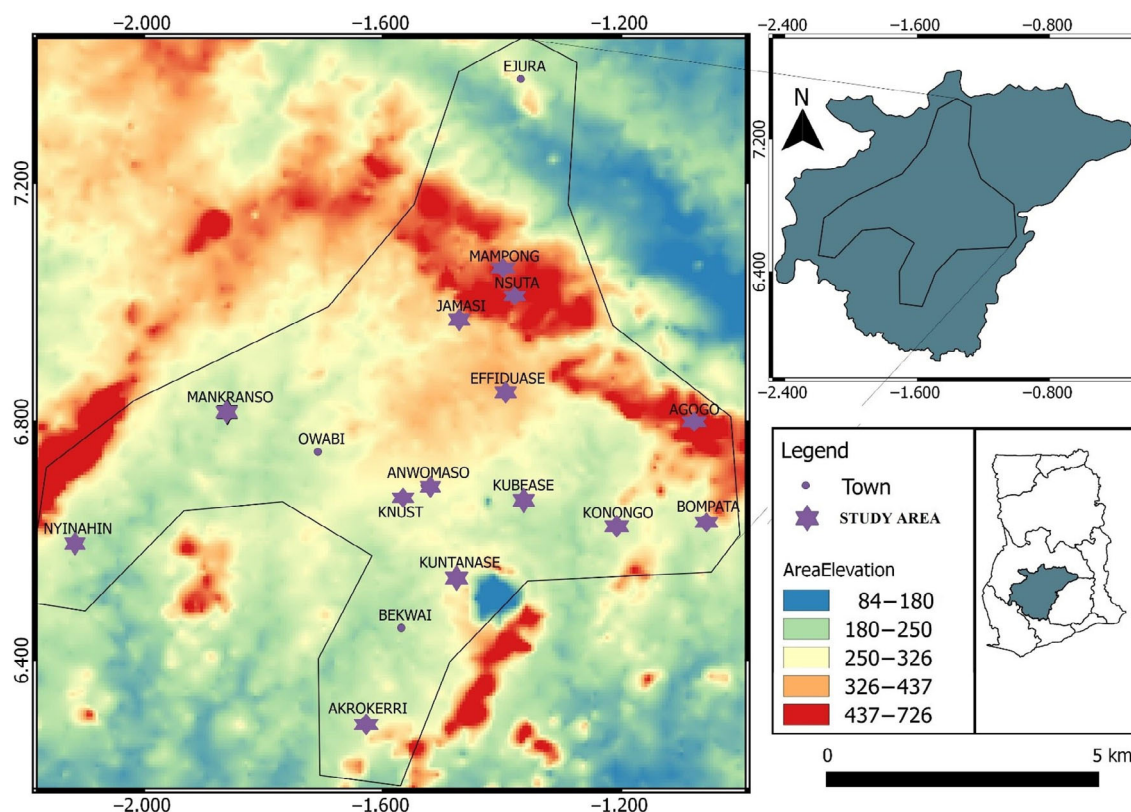


FIGURE 2 Location of optical rain gauge network over the Ashanti Region of Ghana shown by stars (modified from Amekudzi et al., 2016).

was tested. The day was selected for the atmospheric profile verification due to the availability of in situ data on 17 June, 2016. The ERA5 rainfall, relative humidity, and wind speed and direction (u- and v-components) were used to study the meteorological conditions of the surface to the 200 hPa level in the atmosphere. Studies (e.g., Meukaleuni et al., 2016; Olauson, 2018; Panitz et al., 2014; Sylla et al., 2010) have employed ERA-INTERIM and ERA5 in climate analysis and found them suitable over the globe and West Africa. Further information on these products is given by Berrisford et al. (2009) and Hersbach et al. (2020). In this study, hourly rainfall accumulations are used for the verification of the severe storm in Kumasi on the 28 June, 2018.

2.5 | CHIRPS dataset

The Climate Hazards Group Infrared Precipitation combined with Station Data (CHIRPS) is a quasi-global precipitation product with a horizontal resolution of $0.05^\circ \times 0.05^\circ$. The data period is from 1981 to present (Peterson et al., 2013). CHIRPS daily rainfall data for all of 28 June were used for the case study analyses. The CHIRPS data have been shown to have good agreement with in situ

rainfall data over West Africa in studies such as Atiah, Amekudzi, et al. (2020) and Dembélé and Zwart (2016).

2.6 | Statistical analysis using probability of detection, false alarm ratio, and critical success index

The probability of detection (PoD) (Ba & Gruber, 2001; Krajewski et al., 2003), false alarm ratio (FaR) (Nasrollahi, 2015; Wu et al., 2012), and the critical success index (CSI) are used to verify the performance of GPM and ERA5 in identifying storm over the study area on hourly basis using the DACCWA gauge data as reference data. The PoD measures the fraction of the DACCWA gauge rainfall that is detected by GPM and ERA5 data while the FaR measures the fraction of events given by satellites but not captured by the gauges (AghaKouchak et al., 2011). The CSI measures accuracy sensitive to missed events and false alarms. The metrics range from no skill (0) to perfect skill (1). A PoD of one and a FaR of zero mean the data detected exactly as the DACCWA gauge rainfall. These statistics have been used in studies over this region and have proved effective in evaluating rainfall products (AghaKouchak et al., 2011;

Amekudzi et al., 2016; Maranan et al., 2020). The PoD, FaR, and the CSI are given by Equations (2–4), respectively.

$$\text{PoD} = \frac{H}{H + M}, \quad (2)$$

$$\text{FaR} = \frac{F}{H + F}, \quad (3)$$

$$\text{CSI} = \frac{H}{H + F + M}, \quad (4)$$

where H (Hits) is the rain correctly detected by ERA5 and GPM, M (Miss) is the rainfall by DACCIIWA but not detected by ERA5 and GPM, and F (False alarm) is the rain detected by ERA5 and GPM but not by the DACCIIWA.

2.7 | Atmospheric stability analysis

To provide a context of synoptic conditions for the heavy rainfall event, we briefly look at the intensity of the storm by considering the instability before, during, or

after the storm based on observation and other products. The ERA-INTERIM profile data are used as a reference in the absence of ground-based sounding resulting from its performance in reproducing the temperature profile of the atmosphere (with DACCIIWA sounding as observed in Section 2.7.1). For this task, we focus on Convective Available Potential Energy (CAPE), K-index (KI), and Lifted index (LI) (Blanchard, 1998; Galway, 1956; Riemann-Campe et al., 2009; Tyagi et al., 2011) defined in Table 1.

2.7.1 | Evaluation of atmospheric profile datasets

This section shows a brief evaluation of ERA (ERA5 and ERA-INTERIM) and National Centers for Environmental Prediction (NCEP) temperature profiles relative to DACCIIWA radiosonde data. Figure 3 shows the temperature profile for Kumasi on 17 June, 2016 for the DACCIIWA, ERA-INTERIM, ERA5, and NCEP. This day experienced rainfall that led to flooding in some parts of the city. The day is used for evaluation purposes because of the

TABLE 1 The details of the indices used in this study; the CAPE (Blanchard, 1998; Riemann-Campe et al., 2009), K-index (Tyagi et al., 2011), and lifted index (Galway, 1956).

Convective Available Potential Energy	Meaning	KI	Meaning	Lifted index	Meaning
0–1000	Marginally unstable	20–25	Isolated thunderstorm (TS)	>0	No convective activity, showers
1000–2500	Moderately unstable	26–30	Widely scattered TS	–2 to 0	Showers, isolated TS
2500–3500	Very unstable	31–35	Scattered TS	–4 to –2	Thunder storm (TS)
3500+	Extremely unstable	Above 35	Numerous TS	<–4	Severe TS

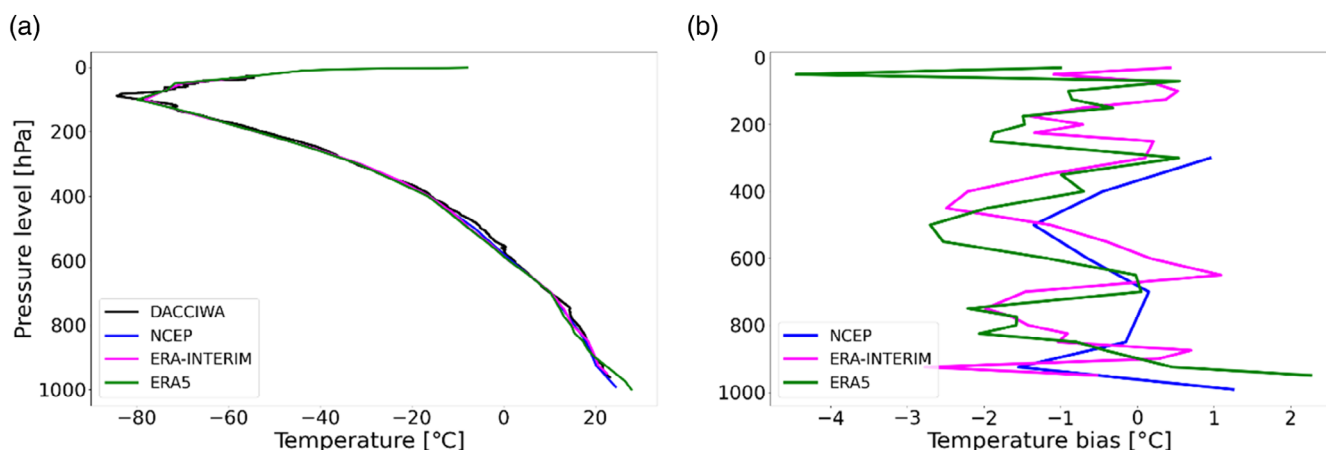


FIGURE 3 The temperature profile of the atmosphere (a) over Kumasi and the difference between NCEP, ERA-INTERIM, and ERA5 and Dynamics–Aerosol–Chemistry–Cloud Interactions in West Africa (DACCIIWA) (b) for 17 June, 2016 shown by DACCIIWA and ERA5.

availability of ground observation data on that day. Additionally, the analysis was done on 17 June, 2016 due to the availability of atmospheric profile data from the DACCIWA project. There were no further atmospheric profile measurements after 2016. Additionally, 17 June, 2016 was used due to the similarities in the characteristics (severe rainfall) of the storms on the 17 June, 2016 and 28 June, 2018. Although this is done for just a single case, it provides the starting point for future studies or analyses when actual in situ observations are available for severe rainfall cases. Here we assessed the temperature profile to analyze the stability of the atmosphere before the rain started, as shown in Figure 3a. All the datasets (ERA-INTERIM, ERA5, and NCEP) captured the atmospheric temperature profile of Kumasi well with biases of $\pm 4.0^{\circ}\text{C}$ (shown in Figure 3b) with ERA5 having the highest bias of -4.0°C near the 100 hPa level. The NCEP data only have levels up to 300 hPa, making it impossible to assess atmospheric temperature profile beyond 300 hPa level.

Determining the available energy for storm initiation, a CAPE value of 3040.1 J (Figure 4a) showed high available energy that enhanced and sustained the formation of the storm. As shown in Figure 4b and summarized in Table 2, the ERA-INTERIM similarly detects a high CAPE value of 2922, slightly lower than that in the same instability regime (3040). Higher CAPE values do not imply the formation of storms; however, with available moisture and appropriate wind dynamics, high CAPE values may

potentially lead to the development of thunderstorms due to high instability (Blanchard, 1998; Riemann-Campe et al., 2009). Hence, the ERA-INTERIM profile dataset was used to assess the atmospheric stability for the severe storm (28 June, 2018) in Kumasi.

2.8 | Temporal analysis of DACCIWA, ERA5, and GPM GPM for the severe flood on 28 June, 2018

The diurnal cycles of rainfall over the network of rain gauges over the study area are analyzed for the 28 June, 2018 case under study. First, the diurnal cycle of rainfall recorded by gauges at the 14 stations are shown under the northern, middle, and southern sectors (Shown in

TABLE 2 CAPE, pressure, and temperature at lifting condensation level for 17 June, 2016 over Kumasi.

	DACCIWA	ERA-INTERIM
CAPE	3040.1 J	2922 J
Pressure at lifting condensation level	885.6	914.0 hPa
Temperature at lifting condensation level	21.3°C	21.0°C

Abbreviation: DACCIWA, Dynamics–Aerosol–Chemistry–Cloud Interactions in West Africa.

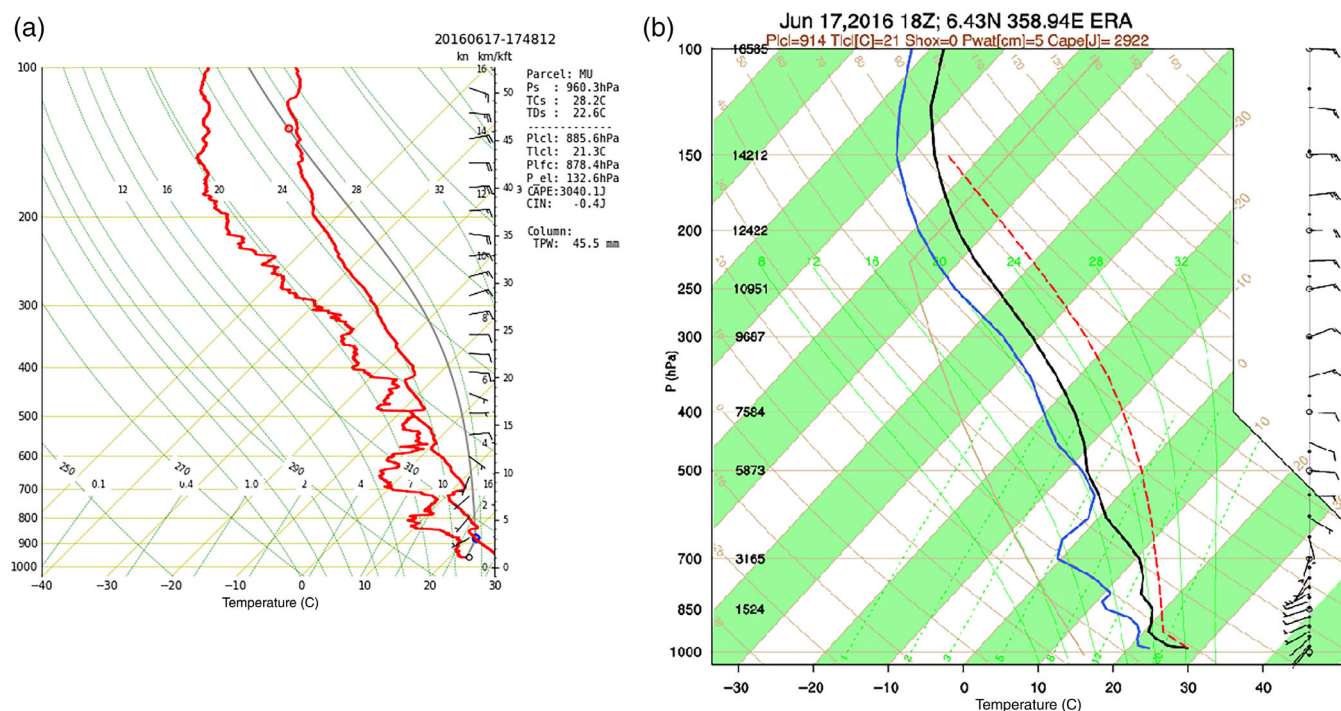


FIGURE 4 The SkewT plots of Dynamics–Aerosol–Chemistry–Cloud Interactions in West Africa (a), and ERA-INTERIM (b) over Kumasi for 17 June, 2016. The plot shows details of instability as shown by CAPE values.

Figure 9). Second, the mean of the rainfall amounts at the stations located within the southern, the middle, and the northern sectors of the study area are computed. The exact grid points (corresponding to longitude and latitude of DACCWA station locations) for GPM and ERA5 were extracted for stations falling under the three sectors and their means were determined and compared with that of DACCWA gauges (shown in Figure 10).

2.9 | Standardized anomaly of rainfall

The standardized anomaly index (SAI) was used to standardized rainfall by assessing the deviation from the mean (Wallace & Hobbs, 2006). The method was used to assess the uniqueness of the 28 June, 2018 rainfall event. SAI is defined by Equation (5)

$$SAI = \frac{x - \bar{x}}{\sigma}, \quad (5)$$

where $x - \bar{x}$ is the deviation of 28 June, 2018, x is obtained from the climatological mean of all 28 June, \bar{x} .

TABLE 3 Standard Anomaly Index (SAI) and the meaning (McKee et al., 1993).

SAI	Meaning
≥ 2.0	Extremely wet (EW)
1.50 to 1.99	Severely wet (SW)
1.00 to 1.49	Moderately wet (MW)
0.99 to -0.99	Near normal (NN)
-1.00 to -1.49	Moderate dry (MD)
-1.50 to -1.99	Severely dry (SD)
≤ -2.0	Extremely dry (ED)



The standard deviation for 1981–2018 period is given by σ . The severity of rainfall is classified using categorization in Table 3.

3 | RESULTS

3.1 | The 28 June, 2018 storm over Kumasi

The rainfall caused flooding on 28 June, 2018 in Kumasi led to loss of lives and destruction of properties. The rains, which begun in the late afternoon, caused the death of eight people and left hundreds displaced according to the Ghana News Agency. Figure 5 shows places of Kumasi with roads submerged and cars immobilized by floods.

This study assesses the start, duration, and intensity of the storm seen from observations, satellite, and other products. First, we discuss the synoptic conditions leading to the formation of the storm. Subsequently, the temporal variation of storms is compared with IMERG-GPM and ERA5. The spatial distribution of rainfall is ascertained for both IMERG-GPM and ERA5.

3.2 | Rainfall accumulation and anomaly

Figure 6 shows the daily accumulation (Figure 6a) and corresponding standardized anomaly (Figure 6b) on 28 June, 2018. The storm was more intense over the western coast (daily accumulation above 70 mm) compared with the middle sector (daily accumulation between 40 and 60 mm). The standardized anomaly indicates rainfall amounts above 3σ above normal, indicating extremely wet event (see Table 3). The anomaly shows the severity of the event relative to the climatological mean for all 28th June, resulting in floods that caused damages to properties in the Ashanti Region.



FIGURE 5 Areas of Kumasi Flooded after the heavy rainfall on 28 June, 2018. Source: citinewsroom.com.

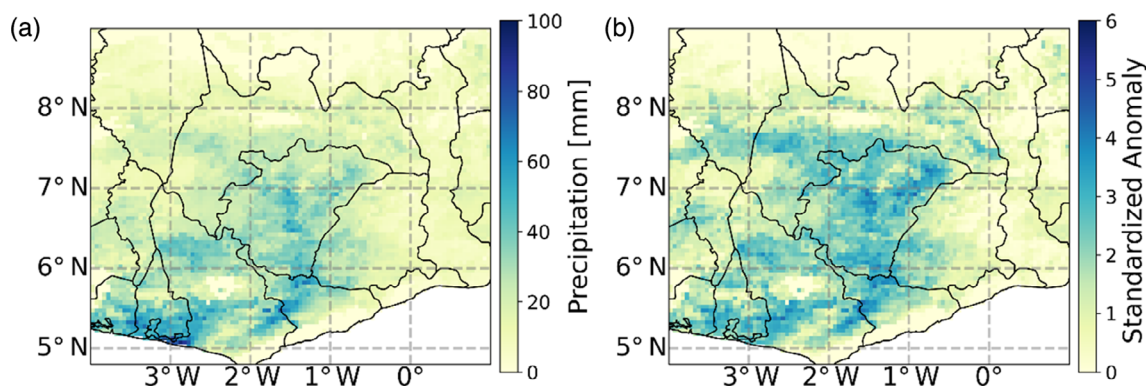


FIGURE 6 Rainfall accumulation (a) from CHIRPS on 28 June, 2018. (b) The standardized anomaly index for 28 June, 2018 relative to the climatological mean for all 28th June, from 1981 to 2018.

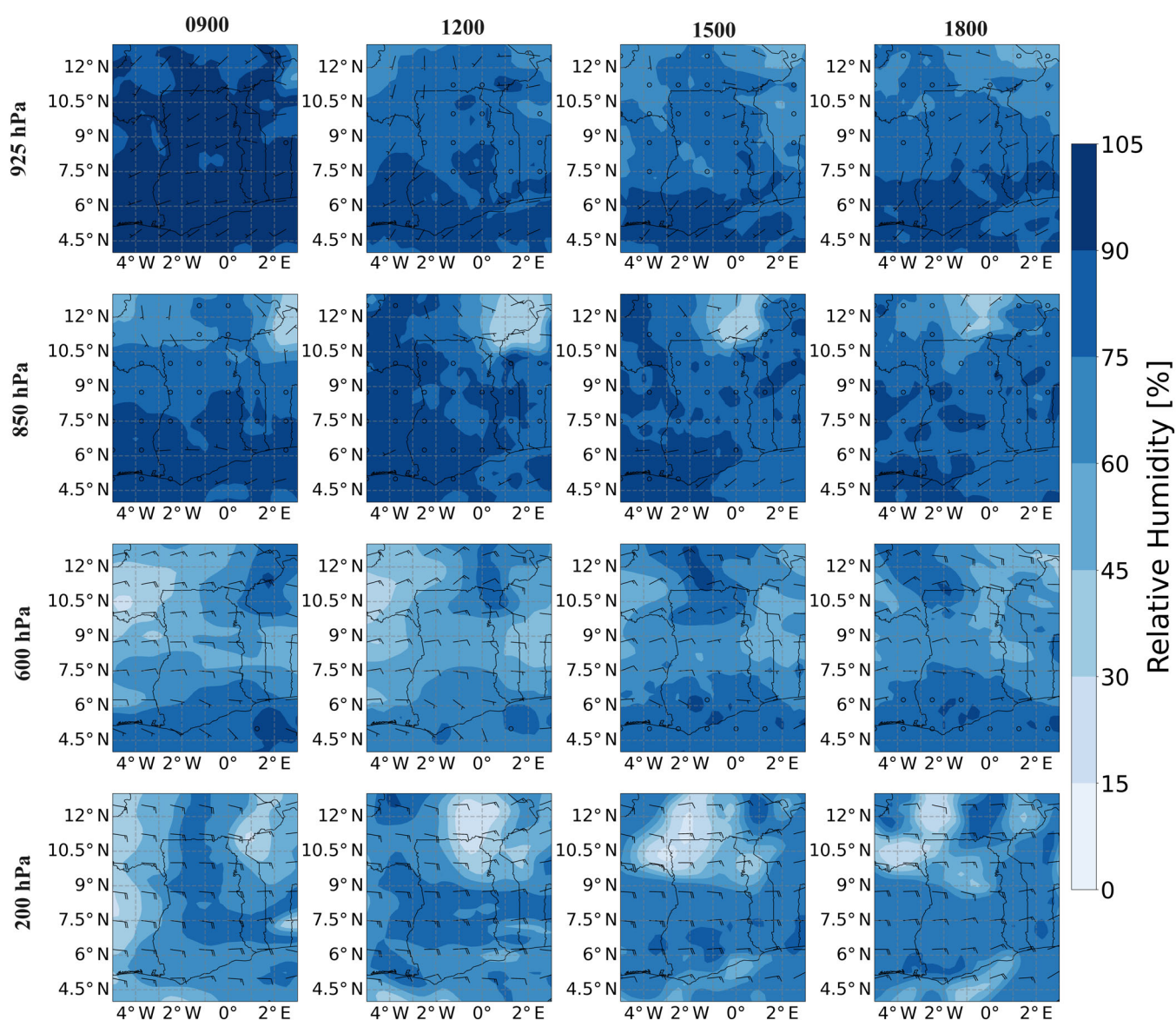


FIGURE 7 Relative humidity and wind at 0900, 1200, 1500, and 1800 (on the horizontal) at 925, 850, 600, and 200 hPa levels (on the vertical) for 28 June, 2018.

3.3 | Synoptic analysis, stability analysis, and spatial analysis for Kumasi, 28 June, 2018

3.3.1 | Synoptic analysis

In this section, we briefly describe the weather conditions that influenced the formation of the storm including relative humidity (RH) and wind at various levels (925, 850, 600, and 200 hPa) for various periods (0900 UTC, 1200 UTC, 1500 UTC, and 1800 UTC) (Figure 7). Assessing these would help determine the moisture depth and the strength of the African Easterly Jet (AEJ) and the Tropical Easterly Jet (TEJ). The storm was a slow-moving, lasting for about 8 h. In the morning, 0900 UTC, winds were predominantly southwesterly, leading moisture from the Gulf of Guinea to Ghana with a mean relative humidity of 78% over the entire country at the 925 hPa level. At the 850 hPa level, calm wind dominated northern Ghana while the southern parts were predominantly southwesterly. At mid (600 hPa) and higher (200 hPa) levels, winds are predominantly easterly with high amounts of moisture at 200 hPa over middle and southern Ghana.

At noon, at the surface (925 hPa), the southwestern portions of Ghana were dominated by southwesterly winds, calm winds at 850 hPa, and easterlies at mid (600 hPa) and higher (200 hPa) levels. This condition dominated the entire region through to late afternoon (1500 UTC) and evening (1800 UTC).

The southwesterly winds aid in the transport of moisture inland from the ocean, thereby increasing the available moisture for convection. High RH (75%–100%) exists at the 850 hPa level at all times, which is essential for enhanced tropical deep convection and storm initiation (Holloway & Neelin, 2009; Parker et al., 2016; Taylor et al., 2010). At the 600 and 200 hPa levels corresponding to the AEJ and TEJ levels (Cook, 1999; Flohn, 1964; Nicholson et al., 2007; Thorncroft et al., 2003), RH remains relatively high (>70%) from 0900 to 1800 Z with easterly wind, with a mean value of approximately 10.3 m/s. These weak winds at these levels suggest the AEJ and TEJ are weak. Similar studies have shown that slow-moving storms result from weak AEJ and TEJ (Ansah et al., 2020; Crook et al., 2019; Omotosho, 2008).

3.3.2 | Atmospheric stability analysis

In addition to wind and RH dynamics, the available energy in the atmosphere is crucial for forming storms

TABLE 4 The stability indices of ERA-INTERIM for 28 June, 2018 over Kumasi.

Time	CAPE	K-index	Lifted index
1200 Z	3680 J	33.5 J	−6.0
1800 Z	2260 J	31.3 J	−4.0

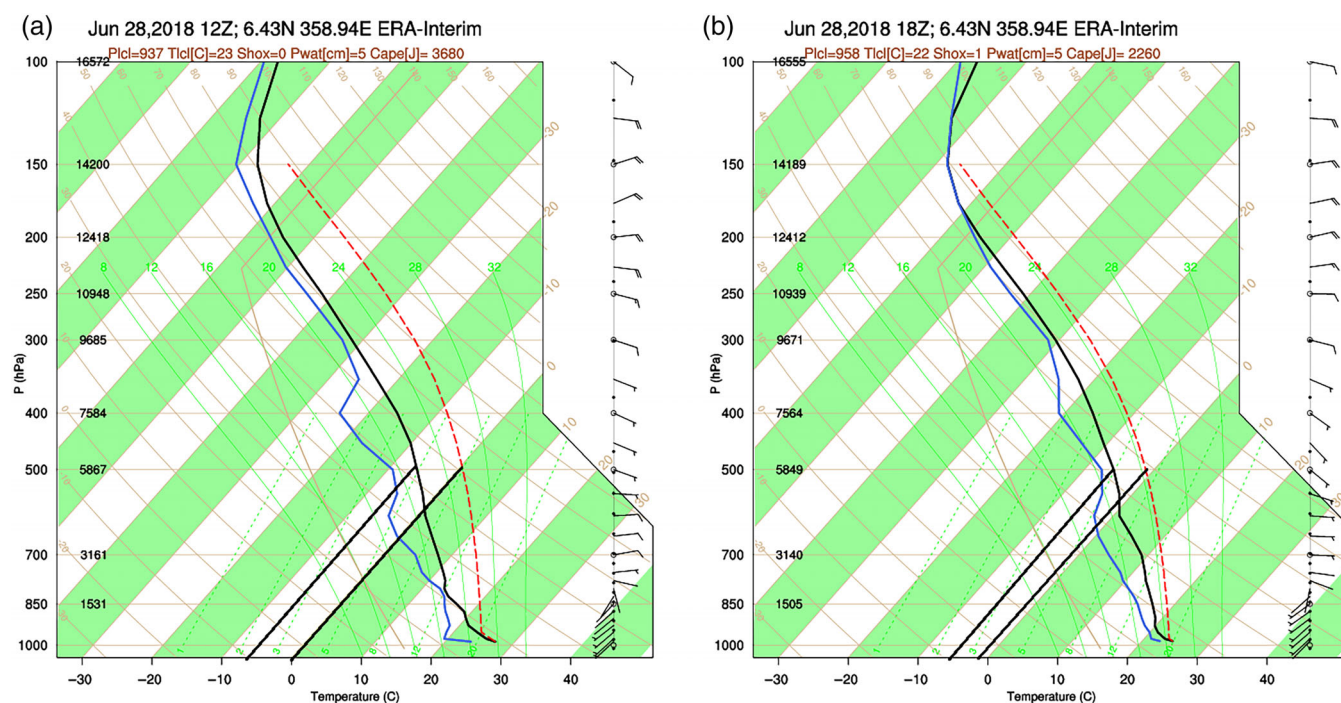


FIGURE 8 The SkewT plots of ERA-INTERIM of Kumasi for 28 June, 2018 showing CAPE and other instability parameters at 1200 UTC and 1800 UTC.

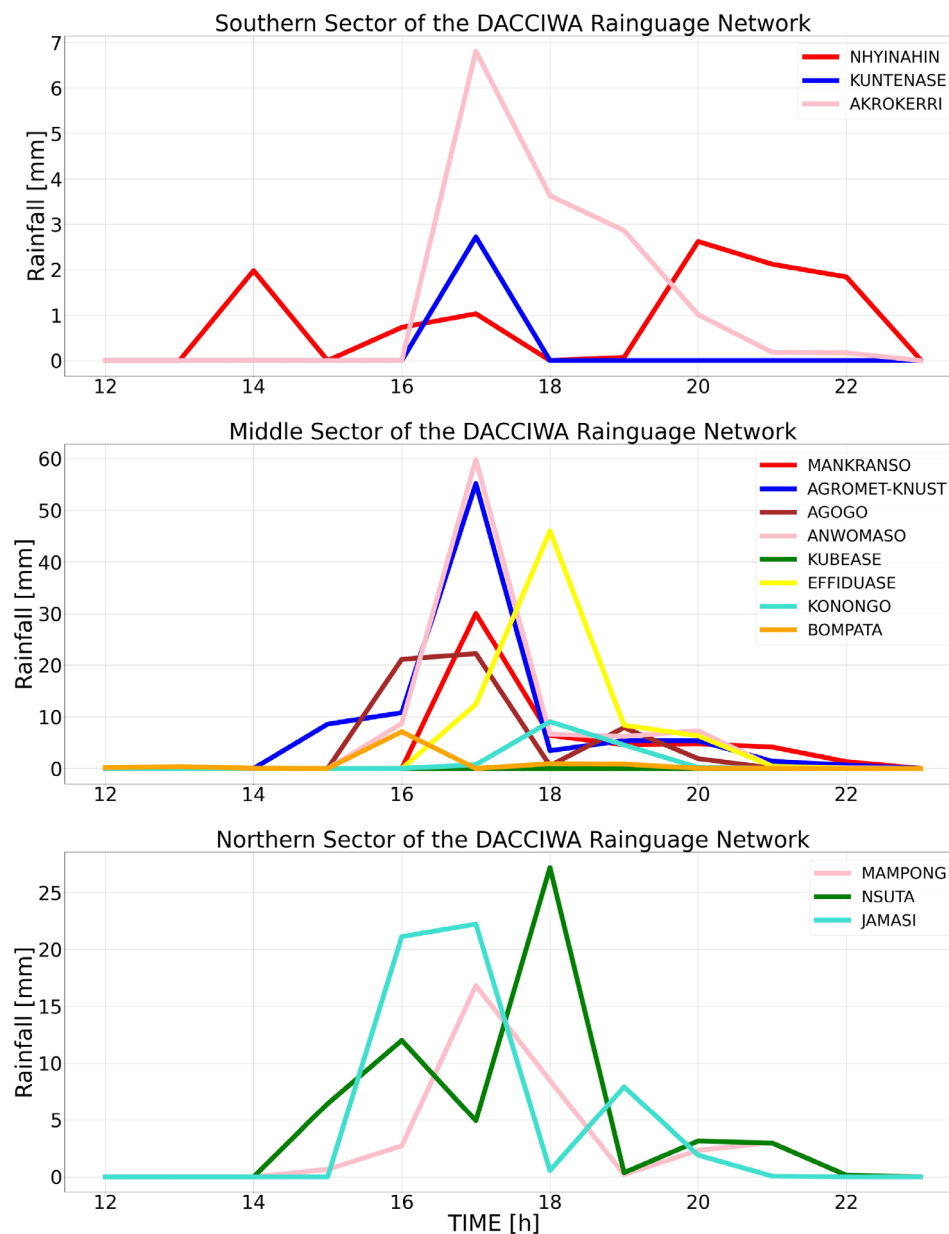


FIGURE 9 Time series of rainfall on 28th June, 2018 at 14 Dynamics-Aerosol-Chemistry-Cloud Interactions in West Africa stations showing rainfall intensities at stations in the southern, middle, and northern sectors.

(Blanchard, 1998; Meukaleuni et al., 2016; Riemann-Campe et al., 2009). The knowledge of the available energy helps forecasters and researchers to know the type of storm to anticipate. Indices such as the CAPE, the KI, and the LI help in determining the available energy. The amount of energy determines the stability of the atmosphere. Figure 8 shows the atmospheric profile over Kumasi at 1200 UTC and 1800 UTC.

Based on the CAPE values (shown in Table 4), we deduce that the atmosphere was highly unstable from noon to 1800 UTC. LI also shows large instability, which indicates that the atmosphere had a lot of energy to support storm formation (Riemann-Campe et al., 2009). Additionally, the KI values indicated the existence of scattered thunderstorms over Kumasi, supporting the idea that the storm developed in a highly unstable atmosphere.

The stability analysis showed that, on 28 June, the atmosphere had enough energy to support thunderstorm formation. This should aid forecasters in knowing the type of storm likely to form and the associated destruction that comes with it. The availability of moisture, deep convection from high CAPE, and favorable winds aided in the development and sustenance of the storm.

3.4 | Precipitation characteristics

3.4.1 | Temporal analysis: Gauge data

In this section, we analyze the diurnal cycle of rainfall over the network of rain gauges over the study area. The rainfall recorded by gauges at the 14 stations shown in

FIGURE 10 Time series of rainfall on 28 June, 2018 from 1200 to 2300 UTC, showing periods of intense rainfall and displaying the mean values from stations in the southern, middle, and northern sectors for Dynamics–Aerosol–Chemistry–Cloud Interactions in West Africa (black), ERA5 (red), and the Global Precipitation Measurement (blue).

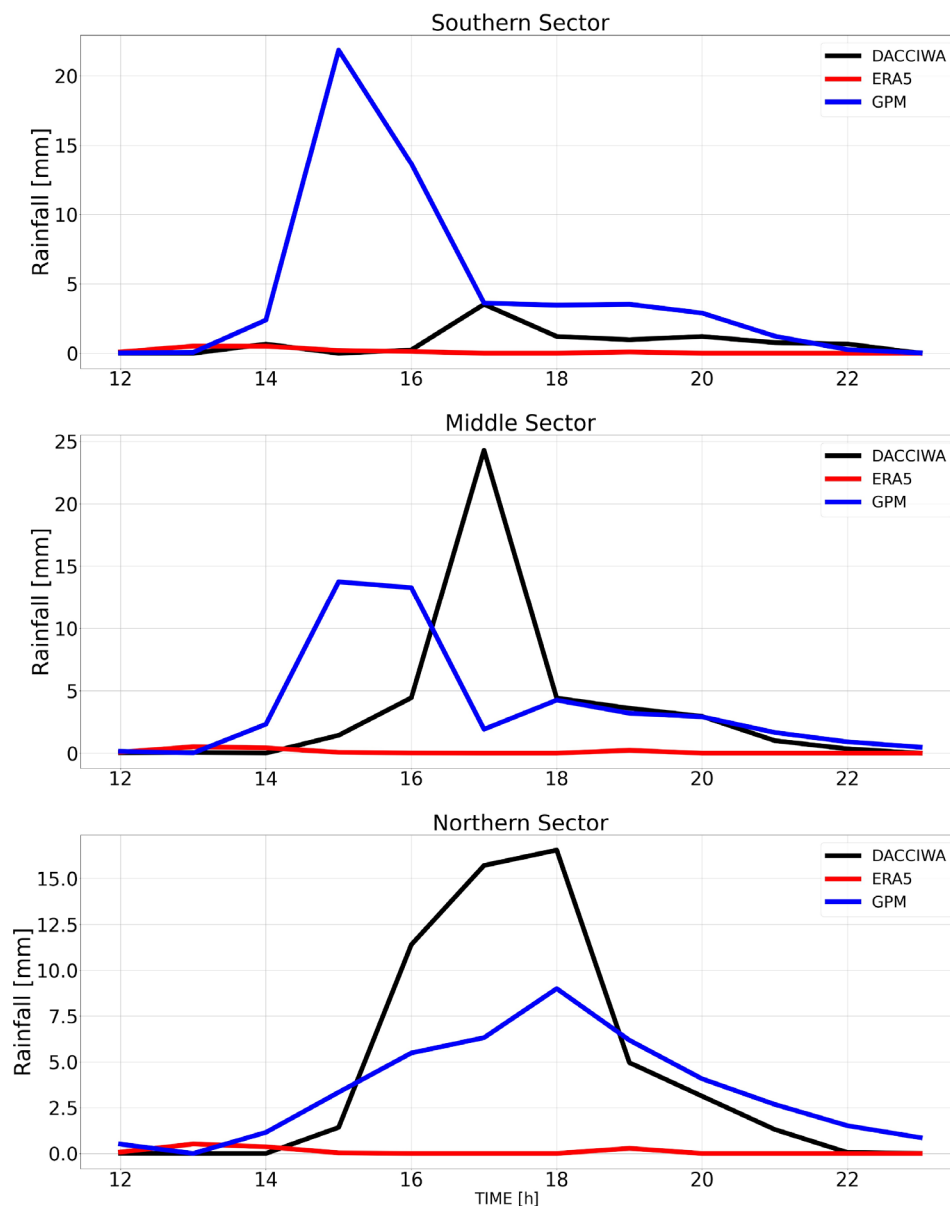


Figure 9 shows the diurnal variation for stations under the gauge network's northern, middle, and southern sectors. An average of rainfall accumulations over the stations in each sector is calculated and plotted against that of GPM and ERA5 (shown in Figure 10). Table 5 shows the daily accumulation from all stations. From the rainfall variations at the various stations, heavy rain began in the southern sector; at Nyinahin (around 1400 UTC). The highest amount of rainfall was recorded in the middle section (more than 90 mm), followed by the northern section, and the lowest amounts in the southern section (shown in Table 5). Based on the results, the bulk of rainfall was recorded within the first 3 h of the start of the rain, which characterizes convective storms over the region. Normally, they are formed as a result of intense convection in the afternoons, producing heavy rainfall

over long hours (Zhang et al., 2021). The intense rainfall over a short period of time, coupled with poor drainage and poor settlement, results in flooding over southern part of Ghana (Karley, 2009).

Figure 10 shows the diurnal variation of rainfall depicted by the DACCIWA gauges, the GPM, and the ERA5 rain on 28 June, 2018. Here, we show the mean of rainfall amounts at the stations located within the southern, middle, and northern sectors of the study area. The corresponding gridded data for each gauge station were extracted by taking the nearest grid point of the GPM and ERA5 datasets. Then, the mean for each sector was calculated from the stations falling in the specific sectors.

The results showed that the GPM showed an early start of the 28th June storm over the northern, middle, and southern sectors. However, the bulk amount of rainfall was

TABLE 5 Daily rainfall accumulation over all 14 Dynamics–Aerosol–Chemistry–Cloud Interactions in West Africa gauge stations, showing the rainfall amounts and various sectors each station falls under.

Station	Rainfall (mm)
North	
Mampong	34.4
Jamasi	57.1
Nsuta	57.9
Middle	
AgroMet-KNUST	90.9
Anwomaso	89.2
Effiduase	80.3
Agogo	57.1
Bompata	9.6
Konongo	14.8
Mankranso	51.6
Kubease	0.0
South	
Akrokerri	14.7
Nyinahin	10.4
Kuntense	2.7

seen within the first 3 h after 1300 UTC. Cold clouds, sometimes perceived as rainfall (Amorati et al., 2000; Xu et al., 2013), significantly influenced the performance of the GPM in capturing rainfall amounts and may be the reason for the early start of the storm.

Studies (Meukaleuni et al., 2016; Olauson, 2018) have shown the robust performance of the ERA5 in reproducing observed precipitation over Africa; however, the ERA5 underestimated the extreme rainfall over the three sectors. Reanalysis rainfall products over the years have expressed the inability to accurately capture the highly variable nature of rainfall over West Africa (Manzanas et al., 2014). This may be due to biases in input models and their inability to capture surface features such as vegetation and orography that influence rainfall.

3.4.2 | Statistical analysis using the PoD, FaR, and CSI

These statistics are used to determine the suitability of GPM and ERA5 in identifying storm hits and misses over the southern, the middle, and the northern sections of the study area using the DACCWA gauge data as reference data. Table 6 gives the 24-h rainfall accumulation PoD and CSI gives the accuracy of the products. Overall,

TABLE 6 Probability of detection (PoD), false alarm ratio (FaR), and critical success index (CSI) used to determine the suitability of Global Precipitation Measurement (GPM) and ERA5 in reproducing hourly rainfall accumulation.

	PoD	FaR	CSI
South			
GPM	0.90	0.31	0.64
ERA5	0.30	0.57	0.21
Middle			
GPM	0.75	0.25	0.60
ERA5	0.38	0.14	0.35
North			
GPM	0.59	0.09	0.56
ERA5	0.18	0.50	0.15

the GPM had high skill in the sectors compared with the ERA5. Over the southern sector, the GPM, shows a PoD, FaR, and CSI of 0.9, 0.31, and 0.64, respectively, whereas the ERA5 gives PoD, FaR, and CSI of 0.3, 0.57, and 0.21, respectively. Over the middle sector, GPM gives PoD of 0.75, FaR of 0.25, and CSI of 0.60. For ERA5, the PoD, FaR, and CSI were 0.38, 0.14, and 0.35, respectively. Over the northern sector, for GPM, PoD, FaR, and CSI were 0.59, 0.09, and 0.56, respectively, whereas PoD, FaR, and CSI for ERA5 were 0.18, 0.5, and 0.15, respectively. Compared with ERA5, the GPM had more hits and hence higher PoD and CSI values. Generally, the GPM and ERA5 did relatively well over the southern portion and performed poorly over the northern sector. This could possibly be due to the fewer stations over the northern sector, resulting in more misses whenever the exact location of the storm is missed. Thiemi et al. (2012); Young et al. (2014), and Amekudzi et al. (2016) have also shown the robustness of satellite products in capturing the variability of rainfall from both cold and warm clouds (Maranan et al., 2020).

3.4.3 | Spatial distribution of daily accumulation of rainfall from ERA5 and GPM

This section looks at the spatial distribution of rainfall for 28 June, 2018, focusing on the daily accumulation (Figure 11) and 3-hourly accumulations for both ERA5 (Figure 12) and GPM (Figure 13). We overlaid the daily accumulations for DACCWA over the location of the stations to check the location of the storm. The spatial distribution depicted by ERA5 shows high amounts of rainfall over the southern portions of the Ashanti Region of Ghana. This could be due to ERA5's ability to simulate

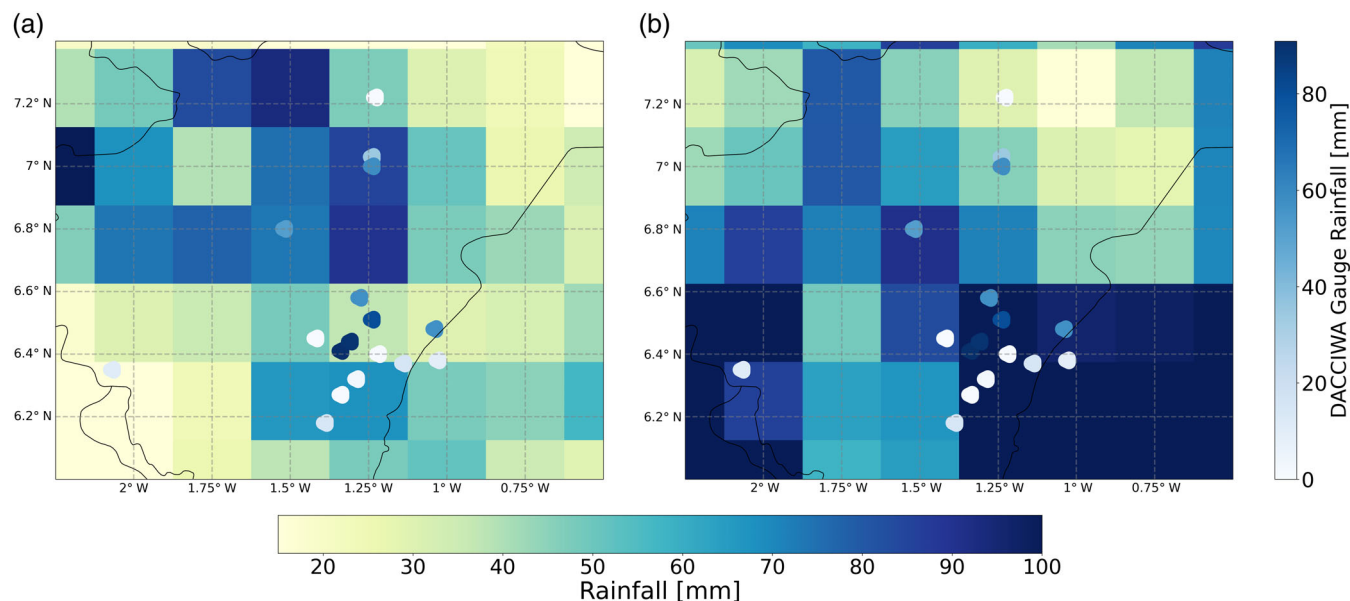


FIGURE 11 Daily accumulation of rainfall for 28 June, 2018 for Global Precipitation Measurement (a) and ERA5 (b). The figure also shows the daily accumulations by all 14-gauge stations.

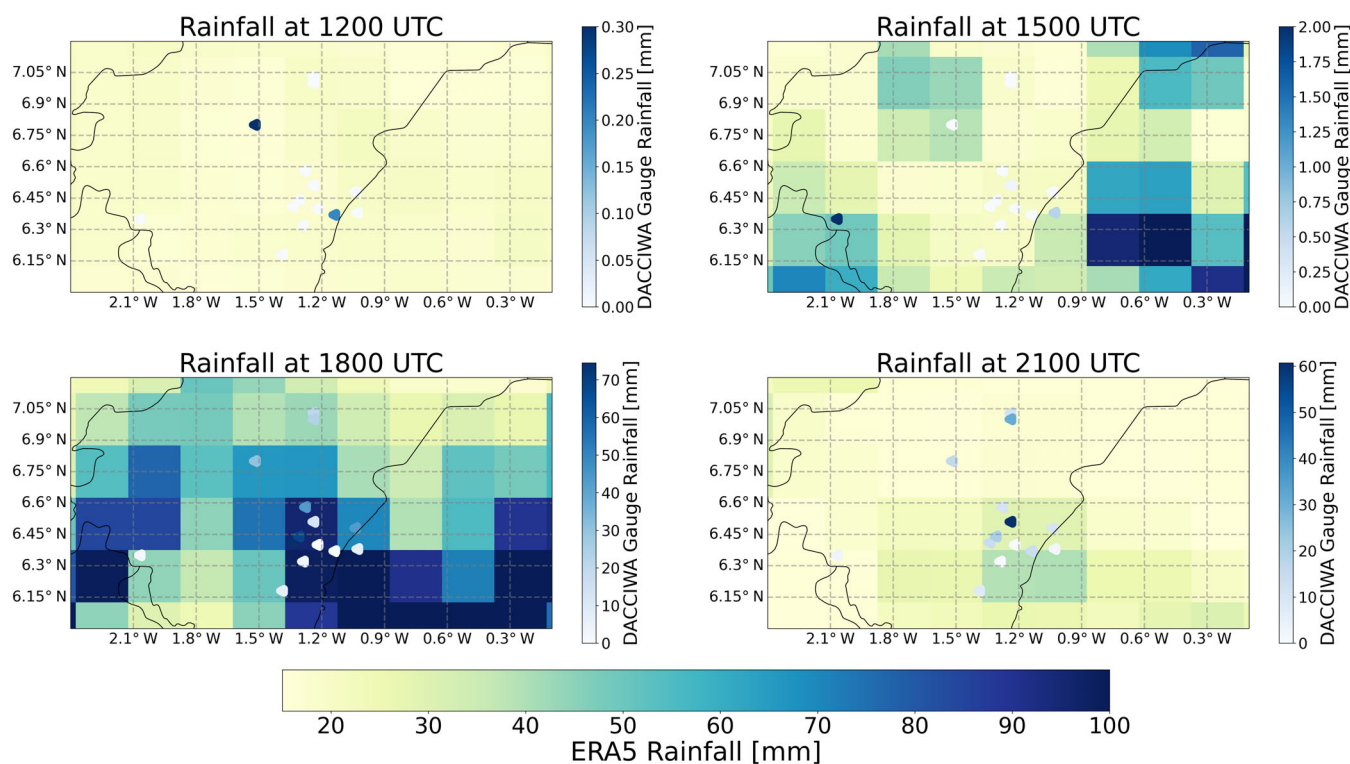


FIGURE 12 Spatial distribution over the Ashanti Region for 28 June, 2018 captured by the ERA5. The figure also shows the 3-hourly accumulations by all 14-gauge stations.

rainfall associated with synoptic scale cyclonic vortices, which may dominate the south due to high moisture availability in the south (Meukaleuni et al., 2016; Olason, 2018). The opposite is seen for GPM showing high

amounts over the northern portions. The use of models in the ERA5 limits its ability to reproduce convective systems partly from course grids (Agyekum et al., 2018; Piani et al., 2010). GPM, on the other hand, gives a more realistic

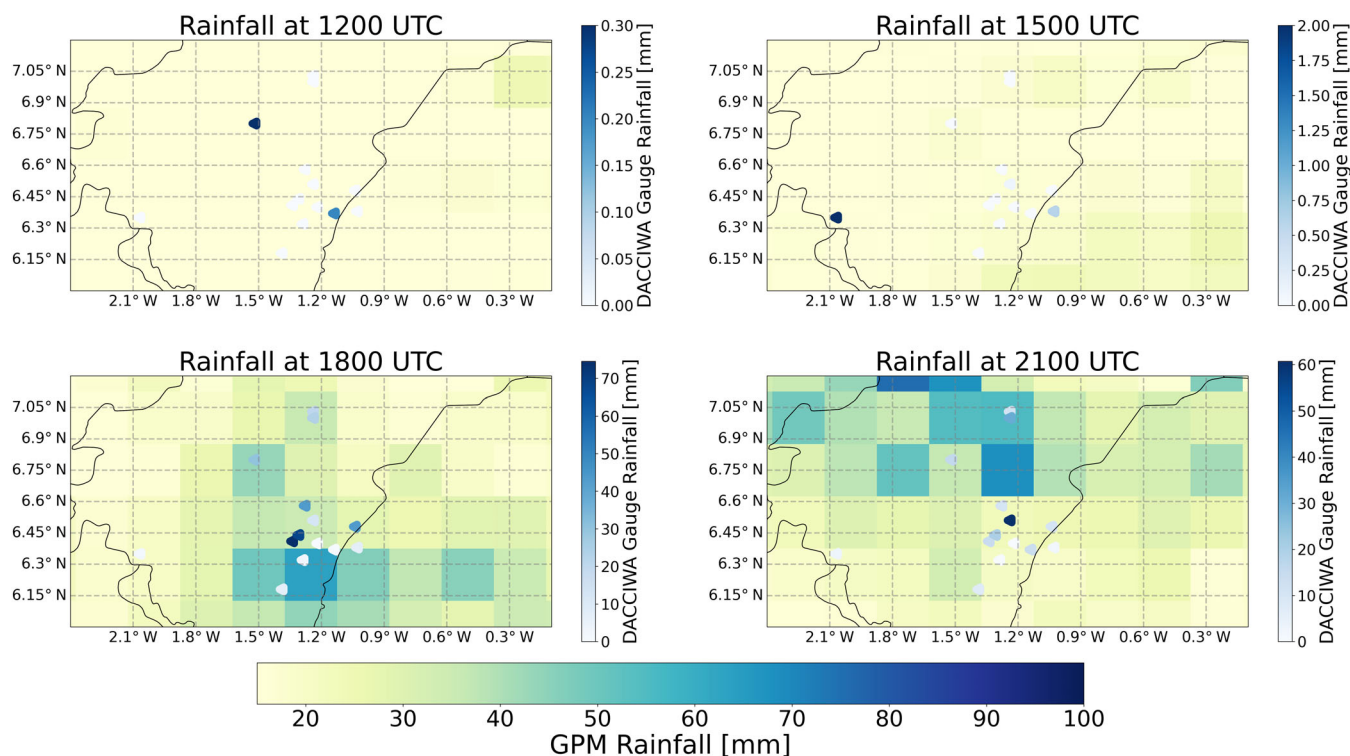


FIGURE 13 Spatial distribution over the Ashanti Region for 28 June, 2018 captured by the Global Precipitation Measurement. The figure also shows the 3-hourly accumulations by all 14-gauge stations.

distribution of rainfall over the area of study. The high spatial resolution of the GPM helps provide a better representation of convective systems (Maranan et al., 2020; Tang et al., 2020).

3.4.4 | Spatial distribution of 3-hourly accumulation of rainfall from ERA5 and GPM

The 3-hourly accumulation from ERA5 (Figure 12) shows rainfall at the southeastern corridors of the study area, which gradually builds up over the southeastern portions of the study area at 1800 UTC and reduces to a minimum over the entire region at 2100 UTC. There is an observed rainfall distribution over the northeast of the study area at 1200 UTC, which increases at 1500 UTC. Maximum spatial coverage and amount of rainfall are observed after 1500 UTC and continue through 2100 UTC. The ERA5 generally placed the areas of maximum rainfall in the southern part of the study area and underestimated the accumulated rainfall. The GPM shows robust details due to finer grid size (see Figure 13). Generally, GPM placed the areas of maximum rainfall over the northern parts of the study area.

4 | CONCLUSIONS

This study sought to look at the storm's characteristics over the Ashanti using rain gauge networks, satellite, and reanalysis data. This study is unique because it employs rain gauge data to assess the onset, duration, and end of a storm in Kumasi. The study is part of the GCRF African Science for Weather Information and Forecasting Techniques (SWIFT) project, which aims to evaluate forecasts and forecast outputs to improve forecasting in East and West Africa. The rainfall that caused flooding in Kumasi and its surrounding areas on 28 June, 2018, claimed lives and destroyed properties. The DACCIWA rain gauges assess the storm's start, duration, and end. Subsequently, the ERA5 and the GPM were analyzed to evaluate their performance in capturing the storm.

The results showed that the rainfall started late afternoon (around 15:45 Z) and lasted until night (around 22:00 Z). The continuous downpour saturated the ground, which caused floods. Coupled with poor settlement planning in the city, the effect of the floods was augmented. The GPM captured the beginning of the storm but underestimated the amount of rainfall accumulation for the day. ERA5 underestimated the daily rainfall over the study area. Both GPM and the ERA5

had difficulty reproducing the hourly pattern of the rain. However, the GPM produced variability that is similar to the observed. Spatially, in general, the region of maximum rainfall was located in the southern parts of the study domain in ERA5, while GPM placed it in the northern parts.

The study has identified data from the DACCWA rain gauges as a valuable dataset for storm characteristics and extreme weather and climate. However, these rain gauges are not available in all meteorological stations in the country. Increasing the density of these gauges in Ghana and West Africa will help improve reliable forecasts and enhance climate studies. Enhancing models' ability to capture these storms will improve the estimates over Ghana, West Africa, and Africa, as weather forecasting in the region relies on these models. Hence, a relatively good model will produce a fair and improved forecast.

AUTHOR CONTRIBUTIONS

Jacob Agyekum: Conceptualization (equal); data curation (equal); formal analysis (lead); investigation (lead); methodology (lead); software (lead); visualization (lead); writing – original draft (lead). **Leonard K. Amekudzi:** Conceptualization (equal); funding acquisition (lead); methodology (equal); supervision (lead); writing – review and editing (equal). **Thorwald Stein:** Conceptualization (equal); methodology (equal); supervision (equal); visualization (equal); writing – review and editing (equal). **Jefrey N. A. Aryee:** Visualization (equal); writing – review and editing (equal). **Winifred Ayinpogbilla Atiah:** Writing – review and editing (equal). **Elijah Adesanya Adefisan:** Writing – review and editing (equal). **Sylvester K. Danuor:** Project administration (equal); writing – review and editing (equal).

ACKNOWLEDGEMENTS

The authors would like to acknowledge the GCRF African SWIFT project for funding this research. This work was supported by UK Research and Innovation as part of the Global Challenges Research Fund, grant number NE/P021077/1. We acknowledge the DACCWA project, European Centre for Medium-Range Weather Forecasts (ECMWF) and National Aeronautics and Space Administration (NASA) for the provision of data used in this study.

FUNDING INFORMATION

This work was supported by UK Research and Innovation as part of the Global Challenges Research Fund, grant number NE/P021077/1.

CONFLICT OF INTEREST STATEMENT

The authors declare no conflicts of interests.

DATA AVAILABILITY STATEMENT

DACCWA rain gauge: The raw rainfall data used in the present study are available under <https://doi.org/10.6096/baobab-dacciwa.1772>. CHIRPS: Data used are available at <https://www.chc.ucsb.edu/data/chirps>. GPM IMERG: Data used for the article are available at <https://gpm.nasa.gov/data/imergr>. ERA5: The data used in this study are available at <https://cds.climate.copernicus.eu#!/search?text=ERA5&type=dataset>.

ORCID

Jacob Agyekum  <https://orcid.org/0000-0001-7484-5338>

Thorwald Stein  <https://orcid.org/0000-0002-9215-5397>

Elijah Adesanya Adefisan  <https://orcid.org/0000-0003-3339-5195>

REFERENCES

- Ageet, S., Fink, A.H., Maranan, M., Diem, J.E., Hartter, J., Ssali, A.L. et al. (2022) Validation of satellite rainfall estimates over equatorial East Africa. *Journal of Hydrometeorology*, 23, 129–151.
- AghaKouchak, A., Behrangi, A., Sorooshian, S., Hsu, K. & Amitai, E. (2011) Evaluation of satellite-retrieved extreme precipitation rates across the Central United States. *Journal of Geophysical Research: Atmospheres*, 116, D02115. <https://doi.org/10.1029/2010JD014741>
- Agyekum, J., Annor, T., Lamptey, B., Quansah, E. & Agyeman, R.Y.K. (2018) Evaluation of cmip5 global climate models over the Volta basin: precipitation. *Advances in Meteorology*, 2018, 1–24.
- Amekudzi, L.K., Osei, M.A., Atiah, W.A., Aryee, J.N., Ahiataku, M.A., Quansah, E. et al. (2016) Validation of trmm and fews satellite rainfall estimates with rain gauge measurement over Ashanti region, Ghana. *Atmospheric and Climate Sciences*, 6, 500.
- Amorati, R., Alberoni, P., Levizzani, V. & Nanni, S. (2000) Ir-based satellite and radar rainfall estimates of convective storms over northern Italy. *Meteorological Applications*, 7, 1–18.
- Ansah, S., Ahiataku, M., Yorke, C., Otu-Larbi, F., Yahaya, B., Lamptey, P. et al. (2020) (2020) meteorological analysis of floods in Ghana. *Advances in Meteorology*, 2020, 1–14.
- Antwi-Agyei, P., Fraser, E.D., Dougill, A.J., Stringer, L.C. & Simelton, E. (2012) Mapping the vulnerability of crop production to drought in Ghana using rainfall, yield and socioeconomic data. *Applied Geography*, 32, 324–334.
- Aryee, J., Amekudzi, L., Quansah, E., Klutse, N., Atiah, W. & Yorke, C. (2018) Development of high spatial resolution rainfall data for Ghana. *International Journal of Climatology*, 38, 1201–1215.
- Asumadu-Sarkodie, S., Owusu, P.A. & Rufangura, P. (2015) Impact analysis of flood in Accra, Ghana. *Advances in Applied Science*. <https://doi.org/10.5281/ZENODO.812994>
- Atiah, W.A., Amekudzi, L.K., Aryee, J.N.A., Preko, K. & Danuor, S.K. (2020) Validation of satellite and merged rainfall data over Ghana, West Africa. *Atmosphere*, 11, 859.
- Atiah, W.A., Tsidu, G.M., Amekudzi, L. & Yorke, C. (2020) Trends and interannual variability of extreme rainfall indices over Ghana, West Africa. *Theoretical and Applied Climatology*, 140, 1–15.

- Ba, M.B. & Gruber, A. (2001) Goes multispectral rainfall algorithm (GMSRA). *Journal of Applied Meteorology*, 40, 1500–1514.
- Banta, R.M. & Barker Schaaf, C. (1987) Thunderstorm genesis zones in the Colorado rocky mountains as determined by trace-back of geosynchronous satellite images. *Monthly Weather Review*, 115, 463–476.
- Berrisford, P., Dee, D., Fielding, K., Fuentes, M., Kallberg, P., Kobayashi, S. et al. (2009) The era-interim archive. *ERA Report Series*, Technical Report. European Centre for MediumRange Forecasts, Shinfield Park, Reading pp. 1–16. <https://doi.org/10.5281/ZENODO.812994>
- Blanchard, D.O. (1998) Assessing the vertical distribution of convective available potential energy. *Weather and Forecasting*, 13, 870–877.
- Browning, K.A., Blyth, A.M., Clark, P.A., Corsmeier, U., Morcrette, C.J., Agnew, J.L. et al. (2007) The convective storm initiation project. *Bulletin of the American Meteorological Society*, 88, 1939–1956.
- Cook, K.H. (1999) Generation of the African easterly jet and its role in determining West African precipitation. *Journal of Climate*, 12, 1165–1184.
- Crook, J., Klein, C., Folwell, S., Taylor, C.M., Parker, D.J., Stratton, R. et al. (2019) Assessment of the representation of West African storm lifecycles in convection-permitting simulations. *Earth and Space Science*, 6, 818–835.
- Dembélé, M. & Zwart, S.J. (2016) Evaluation and comparison of satellite-based rainfall products in Burkina Faso, West Africa. *International Journal of Remote Sensing*, 37, 3995–4014.
- Dinku, T., Ceccato, P. & Connor, S.J. (2011) Challenges of satellite rainfall estimation over mountainous and arid parts of East Africa. *International Journal of Remote Sensing*, 32, 5965–5979.
- Dixon, M. & Wiener, G. (1993) Titan: thunderstorm identification, tracking, analysis, and nowcasting—a radar-based methodology. *Journal of Atmospheric and Oceanic Technology*, 10, 785–797.
- Done, J., Davis, C.A. & Weisman, M. (2004) The next generation of nwp: explicit forecasts of convection using the weather research and forecasting (WRF) model. *Atmospheric Science Letters*, 5, 110–117.
- Finney, D.L., Marsham, J.H., Jackson, L.S., Kendon, E.J., Rowell, D.P., Boorman, P.M. et al. (2019) Implications of improved representation of convection for the East Africa water budget using a convectionpermitting model. *Journal of Climate*, 32, 2109–2129.
- Flohn, H. (1964) *Investigations on the tropical easterly jet*. Environmental Science, Physics. Dümmler.
- Galway, J.G. (1956) The lifted index as a predictor of latent instability. *Bulletin of the American Meteorological Society*, 37, 528–529.
- Gilewski, P. & Nawalany, M. (2018) Inter-comparison of rain-gauge, radar, and satellite (IMERG GPM) precipitation estimates performance for rainfall-runoff modeling in a mountainous catchment in Poland. *Water*, 10, 1665.
- Goudenhoofd, E. & Delobbe, L. (2013) Statistical characteristics of convective storms in Belgium derived from volumetric weather radar observations. *Journal of Applied Meteorology and Climatology*, 52, 918–934.
- Hersbach, H., Bell, B., Berrisford, P., Hirahara, S., Horányi, A., Muñoz-Sabater, J. et al. (2020) The ERA5 global reanalysis. *Quarterly Journal of the Royal Meteorological Society*, 146(730), 1999–2049.
- Holloway, C.E. & Neelin, J.D. (2009) Moisture vertical structure, column water vapor, and tropical deep convection. *Journal of the Atmospheric Sciences*, 66, 1665–1683.
- Huffman, G.J., Bolvin, D.T., Braithwaite, D., Hsu, K., Joyce, R., Xie, P. et al. (2015) Nasa global precipitation measurement (GPM) integrated multi-satellite retrievals for GPM (IMERG). *Algorithm Theoretical Basis Document (ATBD) Version*, 4, 30.
- Huffman, G.J., Bolvin, D.T., Nelkin, E.J. & Tan, J. (2015) Integrated multi-satellite retrievals for GPM (IMERG) technical documentation. *NASA/GSFC Code*, 612, 2019.
- Inness, P.M. & Dorling, S. (2012) *Operational weather forecasting*. Chichester, UK: John Wiley & Sons.
- Karley, N.K. (2009) Flooding and physical planning in urban areas in West Africa: situational analysis of Accra, Ghana. *Theoretical and Empirical Researches in Urban Management*, 4, 25–41.
- Knippertz, P., Coe, H., Chiu, J.C., Evans, M.J., Fink, A.H., Kalthoff, N. et al. (2015) The daccwa project: dynamics–aerosol–chemistry–cloud interactions in West Africa. *Bulletin of the American Meteorological Society*, 96, 1451–1460.
- Krajewski, W.F., Ciach, G.J. & Habib, E. (2003) An analysis of small-scale rainfall variability in different climatic regimes. *Hydrological Sciences Journal*, 48, 151–162.
- Manzanas, R., Amekudzi, L., Preko, K., Herrera, S. & Gutiérrez, J.M. (2014) Precipitation variability and trends in Ghana: an intercomparison of observational and reanalysis products. *Climatic Change*, 124, 805–819.
- Maranan, M., Fink, A.H., Knippertz, P., Amekudzi, L.K., Atiah, W.A. & Stengel, M. (2020) A process-based validation of GPM IMERG and its sources using a mesoscale rain gauge network in the West African forest zone. *Journal of Hydrometeorology*, 21, 729–749.
- McKee, T.B., Doesken, N.J. & Kleist, J. (1993) The relationship of drought frequency and duration to time scales. In: *Proceedings of the 8th Conference on Applied Climatology*, Vol. 17. Boston: American Meteorological Society, pp. 179–183.
- Meukaleuni, C., Lenouo, A. & Monkam, D. (2016) Climatology of convective available potential energy (CAPE) in era-interim reanalysis over West Africa. *Atmospheric Science Letters*, 17, 65–70.
- Mudombi, S. & Nhamo, G. (2014) Access to weather forecasting and early warning information by communal farmers in seke and Murewa districts, Zimbabwe. *Journal of Human Ecology*, 48, 357–366.
- Murray, S.A. (2018) The importance of ensemble techniques for operational space weather forecasting. *Space Weather*, 16, 777–783.
- Nasrollahi, N. (2015) False alarm in satellite precipitation data. In: *Improving infrared-based precipitation retrieval algorithms using multi-spectral satellite imagery*. Ann Arbor, MI: Springer, pp. 7–12.
- Nero, B.F., Callo-Concha, D., Anning, A. & Denich, M. (2017) Urban green spaces enhance climate change mitigation in cities of the global south: the case of Kumasi, Ghana. *Procedia Engineering*, 198, 69–83.
- Nesbitt, S.W., Zipser, E.J. & Kummerow, C.D. (2004) An examination of version-5 rainfall estimates from the trmm microwave imager, precipitation radar, and rain gauges on global, regional, and storm scales. *Journal of Applied Meteorology*, 43, 1016–1036.
- Nicholson, S., Barcion, A., Challa, M. & Baum, J. (2007) Wave activity on the tropical easterly jet. *Journal of the Atmospheric Sciences*, 64, 2756–2763.

- Olauson, J. (2018) Era5: the new champion of wind power modeling? *Renewable Energy*, 126, 322–331.
- Omotosh, J.B. (2008) Pre-rainy season moisture build-up and storm precipitation delivery in the West African Sahel. *International Journal of Climatology: A Journal of the Royal Meteorological Society*, 28, 937–946.
- Owusu, K. & Waylen, P.R. (2013) The changing rainy season climatology of mid-Ghana. *Theoretical and Applied Climatology*, 112, 419–430.
- Panitz, H.-J., Dosio, A., Büchner, M., Lüthi, D. & Keuler, K. (2014) COSMO-CLM (CCLM) climate simulations over CORDEX-Africa domain: analysis of the ERA-interim driven simulations at 0.44 and 0.22 resolution. *Climate Dynamics*, 42, 3015–3038.
- Parker, D.J., Willetts, P., Birch, C., Turner, A.G., Marsham, J.H., Taylor, C.M. et al. (2016) The interaction of moist convection and mid-level dry air in the advance of the onset of the Indian monsoon. *Quarterly Journal of the Royal Meteorological Society*, 142, 2256–2272.
- Peterson, P., Funk, C., Husak, G., Pedreros, D., Landsfeld, M., Verdin, J. et al. (2013) The climate hazards group infrared precipitation (chirp) with stations (chirps): development and validation. *AGU Fall Meeting Abstracts*, 2013, H33E–H1417E.
- Piani, C., Haerter, J. & Coppola, E. (2010) Statistical bias correction for daily precipitation in regional climate models over Europe. *Theoretical and Applied Climatology*, 99, 187–192.
- Quansah, E., Amekudzi, L.K., Preko, K., Aryee, J., Boakye, O.R., Boli, D. et al. (2014) Empirical models for estimating global solar radiation over the Ashanti region of Ghana. *Journal of Solar Energy*, 2014, 1–6.
- Ramsauer, T., Weiß, T. & Marzahn, P. (2018) Comparison of the gpm imerg final precipitation product to radolan weather radar data over the topographically and climatically diverse Germany. *Remote Sensing*, 10, 2029.
- Riemann-Campe, K., Fraedrich, K. & Lunkeit, F. (2009) Global climatology of convective available potential energy (CAPE) and convective inhibition (CIN) in era-40 reanalysis. *Atmospheric Research*, 93, 534–545.
- Sieglauff, J.M., Crounce, L.M., Feltz, W.F., Bedka, K.M., Pavlonis, M.J. & Heidinger, A.K. (2011) Nowcasting convective storm initiation using satellite-based box-averaged cloud-top cooling and cloud-type trends. *Journal of Applied Meteorology and Climatology*, 50, 110–126.
- Stratton, R.A., Senior, C.A., Vosper, S.B., Folwell, S.S., Boutle, I.A., Earnshaw, P.D. et al. (2018) A Pan-African convection-permitting regional climate simulation with the met office unified model: CP4-Africa. *Journal of Climate*, 31, 3485–3508.
- Sun, J., Xue, M., Wilson, J.W., Zawadzki, I., Ballard, S.P., Onvlee-Hoomeyer, J. et al. (2014) Use of nwp for nowcasting convective precipitation: recent progress and challenges. *Bulletin of the American Meteorological Society*, 95, 409–426.
- Sylla, M.B., Coppola, E., Mariotti, L., Giorgi, F., Ruti, P., Dell'Aquila, A. et al. (2010) Multiyear simulation of the African climate using a regional climate model (RegCM3) with the high resolution era-interim reanalysis. *Climate Dynamics*, 35, 231–247.
- Tang, G., Clark, M.P., Papalexio, S.M., Ma, Z. & Hong, Y. (2020) Have satellite precipitation products improved over last two decades? A comprehensive comparison of gpm imerg with nine satellite and reanalysis datasets. *Remote Sensing of Environment*, 240, 111697.
- Taylor, C.M., Harris, P.P. & Parker, D.J. (2010) Impact of soil moisture on the development of a Sahelian mesoscale convective system: a case-study from the amma special observing period. *Quarterly Journal of the Royal Meteorological Society*, 136, 456–470.
- Tengan, C. & Aigbavboa, C.O. (2016) Addressing flood challenges in Ghana: a case of the Accra metropolis.
- Thiemig, V., Rojas, R., Zambrano-Bigiarini, M., Levizzani, V. & De Roo, A. (2012) Validation of satellite-based precipitation products over sparsely gauged African river basins. *Journal of Hydrometeorology*, 13, 1760–1783.
- Thornicroft, C., Parker, D., Burton, R., Diop, M., Ayers, J., Barjat, H. et al. (2003) The jet2000 project: aircraft observations of the African easterly jet and African easterly waves: aircraft observations of the African easterly jet and African easterly waves. *Bulletin of the American Meteorological Society*, 84, 337–352.
- Thorne, V., Coakley, P., Grimes, D. & Dugdale, G. (2001) Comparison of TAMSAT and CPC rainfall estimates with raingauges, for southern Africa. *International Journal of Remote Sensing*, 22, 1951–1974.
- Tyagi, B., Krishna, V.N. & Satyanarayana, A. (2011) Study of thermodynamic indices in forecasting pre-monsoon thunderstorms over Kolkata during storm pilot phase 2006–2008. *Natural Hazards*, 56, 681–698.
- Wallace, J.M. & Hobbs, P.V. (2006) *Atmospheric science: an introductory survey*, Vol. 92. Oxford, UK: Elsevier's Science and Technology.
- Wilson, J.W. & Schreiber, W.E. (1986) Initiation of convective storms at radar-observed boundary-layer convergence lines. *Monthly Weather Review*, 114, 2516–2536.
- Wood, S., Jones, D. & Moore, R. (2000) Accuracy of rainfall measurement for scales of hydrological interest. *Hydrology and Earth System Sciences*, 4, 531–543.
- Wu, H., Adler, R.F., Hong, Y., Tian, Y. & Policelli, F. (2012) Evaluation of global flood detection using satellite-based rainfall and a hydrologic model. *Journal of Hydrometeorology*, 13, 1268–1284.
- Xu, W., Adler, R.F. & Wang, N.-Y. (2013) Improving geostationary satellite rainfall estimates using lightning observations: underlying lightning–rainfall–cloud relationships. *Journal of Applied Meteorology and Climatology*, 52, 213–229.
- Young, M.P., Williams, C.J., Chiu, J.C., Maidment, R.I. & Chen, S.-H. (2014) Investigation of discrepancies in satellite rainfall estimates over Ethiopia. *Journal of Hydrometeorology*, 15, 2347–2369.
- Zhang, X., Shen, W., Zhuge, X., Yang, S., Chen, Y., Wang, Y. et al. (2021) Statistical characteristics of mesoscale convective systems initiated over the Tibetan plateau in summer by fengyun satellite and precipitation estimates. *Remote Sensing*, 13, 1652.

How to cite this article: Agyekum, J., Amekudzi, L. K., Stein, T., Aryee, J. N. A., Atiah, W. A., Adefisan, E. A., & Danuor, S. K. (2023). Verification of satellite and model products against a dense rain gauge network for a severe flooding event in Kumasi, Ghana. *Meteorological Applications*, 30(5), e2150. <https://doi.org/10.1002/met.2150>